# FLUID-STRUCTURAL INTERACTIONS USING NAVIER-STOKES FLOW EQUATIONS COUPLED WITH SHELL FINITE ELEMENT STRUCTURES

Guru P. Guruswamy* and Chansup Byun†
Computational Aerosciences Branch
NASA Ames Research Center, Moffett Field, California 94035-1000

## Abstract

A computational procedure is presented to study fluid-structural interaction problems for three-dimensional aerospace structures. The flow is modeled using the three-dimensional unsteady Euler/Navier-Stokes equations and solved using the finite-difference approach. The three dimensional structure is modeled using shell/plate finite-element formulation. The two disciplines are coupled using a domain decomposition approach. Accurate procedures both in time and space are developed to combine the solutions from the flow equations with those of the structural equations. Time accuracy is maintained using aeroelastic configuration-adaptive moving grids that are computed every time step. The work done by aerodynamic forces due to structural deformations is preserved using consistent loads. The present procedure is validated by computing the aeroelastic response of a wing and comparing with experiment. Results are illustrated for a typical wing-body configuration.

## Introduction

In recent years, significant advances have been made for single disciplines in both computational fluid dynamics (CFD) using finite-difference approaches[1] and computational structural dynamics (CSD) using finite-element methods (see Chapter I of Ref. 2). For aerospace vehicles, structures are dominated by internal discontinuous members such as spars, ribs, panels and bulkheads. The finite-element (FE) method, which is fundamentally based on discretization, has proven to be computationally efficient to solve aerospace structures problems. The external aerodynamics of aerospace vehicles is dominated by field discontinuities such as shock waves and flow separations. Finite-difference (FD) computational methods have proven to be efficient to solve such problems.

Problems in aeroelasticity associated with nonlinear systems have been solved using both uncoupled and coupled methods.[3] Uncoupled methods are less expensive but are limited to very small perturbations with moderate nonlinearity. However, aeroelastic problems of aerospace vehicles are often dominated by large structural deformations and high flow nonlinearities. Fully coupled procedures are required to solve such aeroelastic problems accurately.

In computing aeroelasticity with coupled procedures, one needs to deal with fluid equations in an Eulerian reference system and structural equations in a Lagrangian system. Also, the structural system is physically much stiffer than the fluid system. As a result, the numerical matrices associated with structures are orders of magnitude stiffer than those associated with fluids. Therefore, it is numerically inefficient or even impossible to solve both systems using a monolithic numerical scheme.

Guruswamy and Yang[3] presented a numerically accurate and efficient approach to solve this problem for two-dimensional airfoils by independently modeling fluids using FD-based transonic small perturbation (TSP) equations and structures using FE equations and coupling the solutions only at boundary interfaces between fluids and structures. The coupling of solutions at boundaries can be done either explicitly or implicitly. This domain decomposition approach allows one to take full advantage of numerical procedures of individual disciplines such as FD for fluids and FE for structures. This accurate coupling procedure has been extended to three-dimensional problems and incorporated in several advanced aeroelastic codes such as XTRAN3S[4], ATRAN3S[5] and CAP-TSD[6] based on the TSP theory. It was later demonstrated that the same technique can be used by modeling the fluids with Euler/Navier-Stokes equations on moving grids.[7,8] The accuracy of the coupling is maintained by matching the field grid displacements with the structural displacements at the surface. This new development is incorporated in the computer code ENSAERO.[9]

As an alternate to the domain decomposition approach, there have been some attempts to solve both fluids and structures in a single computational domain.[10,11] This single computational domain approach is not new to the researchers dealing with fluid-

---

* Research Scientist, AIAA Associate Fellow
† Research Scientist, MCAT Institute, AIAA Member

structural interaction problems. In the late 60's, there were several attempts to solve fluid-structural interaction problems using a single FE computational domain (see Chapter 20 of Ref. 12). The main bottleneck arose from ill-conditioned matrices associated with two physical domains with large variations in stiffness properties. As a result, a subdomain approach was devised where fluids and structures are solved in separate domains and solutions are combined through the boundary conditions similar to the domain-decomposition approach explained above. However, there have been renewed attempts to solve both fluids and structures in a single computational domain for aeroelastic applications. So far, such attempts are limited to simple two-dimensional problems and have not proven to be better than the domain decomposition approach. Because of the lack of comparison with other approaches and details about the computational speed, it is difficult to estimate the scope of these alternate approaches. The drop in the convergence rate from the rigid case to the flexible case in Ref. 11 indicates the weakness of the single domain approach.

In the domain decomposition approach, to date, advanced CFD methods such as those based on the Navier-Stokes equations are used to compute aeroelasticity of simple wings modeled structural equations. The modal approach significantly reduces the number of structural unknowns to a great extent when compared to a direct use of FE equations. For simple geometries such as isolated wings, the modal approach can produce accurate response results. However, it can be less accurate for complex structures such as wing-body configurations. Since the structural properties of the body are considerably different from those of the wing, it is difficult to pre-select the modes to accurately represent the full configuration. Therefore, it is more accurate to directly use FE structural equations. Also, by using the FE equations, stresses and other data that are required for the design can be directly computed in addition to displacement responses.

In this work, the capabilities of ENSAERO are extended to compute the aeroelastic responses of general wing-body configurations using the Euler/Navier-Stokes equations for fluids and plate/shell finite-element equations for structures. The coupled equations are solved using a time-integration method with configuration-adaptive moving grids. The results are validated for wings and demonstrated for typical wing-body configurations. Typical aeroelastic responses are computed at transonic Mach numbers.

## Governing Aerodynamic Equations

The strong conservation law form of the Navier-Stokes equations is used for shock capturing purposes. The thin-layer version of the equations in generalized coordinates can be written as[13]

$$\partial_\tau \hat{Q} + \partial_\xi \hat{E} + \partial_\eta \hat{F} + \partial_\zeta \hat{G} = Re^{-1} \partial_\zeta \hat{S} \qquad (1)$$

where $\hat{Q}, \hat{E}, \hat{F}, \hat{G}$, and $\hat{S}$, are flux vectors in generalized coordinates. The following transformations are used in deriving Eq. (1).

$$\begin{aligned} \tau &= t \\ \xi &= \xi(x,y,z,t) \\ \eta &= \eta(x,y,z,t) \\ \zeta &= \zeta(x,y,z,t). \end{aligned} \qquad (2)$$

It should be emphasized that the thin-layer approximation is valid only for high Reynolds number flows, and that very large turbulent eddy viscosities invalidate the model.

To solve Eq. (1), ENSAERO has time-accurate methods based on both central-difference and upwind schemes.[14] In this paper, the central-difference scheme based on the implicit approximate factorization algorithm of Beam and Warming[15] with modifications by Pulliam and Chaussee[16] for diagonalization is used. This scheme is first order accurate in time.

For turbulent flow, the coefficient of viscosity needed for Eq. (1) is modeled using the Baldwin-Lomax algebraic eddy-viscosity model.[17] All viscous computations presented in this paper assume fully turbulent flow. This approximation is consistent with the high Reynolds number assumption. For vortex-dominated flow structures of highly swept wings, a modification to the original Baldwin-Lomax model is required. For this study, the Degani-Schiff modification[18] to the original model for treating vortical flows is used.

## Aeroelastic Equations of Motion

Following the formulation given in Chapter 20 of Ref. 12, the FE matrix form of the aeroelastic equation of motion is

$$[M]\{\ddot{q}\} + [G]\{\dot{q}\} + [K]\{q\} = \{Z\} \qquad (3)$$

where [M], [G], and [K] are the global mass, damping, and stiffness matrices, respectively. $\{Z\}$ is the aerodynamic force vector corresponding to the nodal displacement vector $\{q\}$.

In this work, it is assumed that the wing-body configuration can be modeled using plate/shell elements. For this purpose, it is further assumed that

the structural properties of the body and wing are represented by equivalent shell and plate elements. The ANS4 shell/plate element is used to represent the structural properties of the wing-body configuration.[19] The ANS4 element shown in Fig. 1 is a 20 degrees-of-freedom (DOF) element which can model both plates and shells. It is based on assumed natural strain approach. For the wing-body configuration considered in this work, the wing and the body are modeled using plate and shell options of the ANS4 element, respectively. At each node, the DOF allowed are the inplane displacements $u$ and $v$, transverse deflection ($w$), rotation about x-axis ($\theta$) and rotation about y-axis ($\phi$).

The main effort after selecting the FE model of the structure falls into computing the global force vector $\{Z\}$ of Eq. (4). $\{Z\}$ is computed by solving the Euler/Navier-Stokes Eq. (1) at given time, t. First, the pressures are computed at all surface grid points. The forces corresponding to the nodal DOF are computed using the FE nodal fluid-structural interfaces discussed in the next section.

## Fluid-Structural Interfaces

In aeroelastic analysis, it is necessary to represent equivalent aerodynamic loads at the structural nodal points and to represent deformed structural configurations at the aerodynamic grid points. In the present domain decomposition approach, coupling between the fluid and structural domains is achieved by combining the boundary data such as aerodynamic pressures and structural deflections at each time step. An analytical moving grid technique has been successfully used to deform the aerodynamic grid according to structural deflections at the end of every time step.[7] There are several different ways to obtain the global force vector $\{Z\}$ of Eq. (3) depending on the equations used for the structural dynamic analysis.

A number of numerical procedures have been developed to exchange the necessary information between the aerodynamic and structural domains.[7] A bi-linear interpolation and a virtual-surface interface are used in this study. The bi-linear interpolation is also called the lumped load (LL) approach. In this approach, the force acting on each element of the structural mesh is first calculated, and then the element nodal force vector is obtained by distributing the total force. The global force vector is obtained by assembling the nodal force vectors of each element. In addition, the deformed configuration of the CFD grid at the surface is obtained by linearly interpolating nodal displacements at finite-element nodes. This approach does not conserve the work done by the aerodynamic forces and needs fine grids for both fluids and structures to give accurate results.

An alternate to the above LL approach is an improved approach based on virtual surface (VS). In this approach, a mapping matrix developed by Appa[20] is selected to accurately exchange data between the fluid and structural interface boundaries. The reason for selecting Appa's method is that the mapping matrix is general enough to accommodate changes in fluid and structural models easily. In addition, this approach conserves the work done by aerodynamic forces when obtaining the global nodal force vector. This method introduces a virtual surface between the CFD surface grid and the finite element mesh for the wing. This virtual surface is discretized by a number of finite elements, which are not necessarily the same elements used in the structural surface modeling.

By forcing the deformed virtual surface to pass through the given data points of the deformed structure, a mapping matrix relating displacements at structural and aerodynamic grid points is derived as

$$[T] = [\psi_a]\left(\delta^{-1}[K] + [\psi_s]^T[\psi_s]\right)^{-1}[\psi_s]^T \qquad (4)$$

where

$[K]$: the free-free stiffness of the virtual surface
$\psi_s$: displacement mapping from virtual to structural grids
$\psi_a$: displacement mapping from virtual to aerodynamic grids
$\delta$: penalty parameter

Then, the displacement vector at the aerodynamic grid, $\{q_a\}$, can be expressed in terms of the displacement vector at the structural nodal points, $q_s$, as

$$\{q_a\} = [T]\,\{q_s\}.$$

From the principle of virtual work, the nodal force vector, $\{Z_s\}$, can be obtained as

$$\{Z_s\} = [T]^T\,\{Z_a\}$$

where $\{Z_a\}$ is the force vector at the aerodynamic grids. This procedure is illustrated in Fig. 2.

The aeroelastic equation of motion, Eq. (3), is solved by a numerical integration technique based on the constant-average-acceleration method.

## Aeroelastic Configuration Adaptive Grids

One of the major difficulties in using the Euler/Navier-Stokes equations for computational aerodynamics lies in the area of grid generation. For steady flows,

advanced techniques such as blocked zonal grids[1] are currently being used. However, grid-generation techniques for aeroelastic calculations which involve moving components, are still in the early stages of development. In Ref. 7, aeroelastic configuration adaptive dynamic grids were successfully used for computing time-accurate aeroelastic responses of wings using a C-H grid topology.

In this work, an H-O type grid topology is used (H in the streamwise and O in the spanwise directions) for wing-body configuration. This type of grid topology is more suitable for a general wing-body configurations. It gives better surface grid resolution on the body when compared to the C-H grid topology used in Ref. 7. The base surface grid is generated using the S3D code.[21] From the surface grid, the field grid is generated using an analytical approach. In this approach, grid lines in the radial direction away from the surface are generated line by line in the planes normal to the x-axis. The new grid lines are generated in such a way that the radial lines are approximately normal to the previous line. For example, the first line from the surface is generated such that the radial lines are approximately normal to the surface. In this process the spacing between lines are exponentially increased away from the surface. This base grid is used for computing pressures on the rigid configuration. For aeroelastic analysis, the displacements at structural nodes are computed first using Eq. (3). These displacements are then mapped onto the surface grid points by the interface approach discussed above. Finally the field grid is analytically generated starting from the new deformed surface.

## Results

### Computations on Wing Configuration

To demonstrate aeroelastic computations, a typical fighter type wing of aspect ratio three and taper ratio 1/7 with the NACA 65A006 airfoil section was selected. The sweep angle at the quarter chord line ($\Lambda_{c/4}$) is 45 deg. The transonic flutter characteristics of this wing are available from wind tunnel tests[22] for various flow parameters.

In this computation, the flow field is discretized using a C-H grid topology of size 151 x 30 x 35. The 20 DOF ANS4 shell/plate element[19] was used for the FE modeling of the wing structure. The wing is modeled as a flat plate. Considering the wing structure used in the experiment, variation of mass density is allowed along both chordwise and spanwise directions. However, the thickness of the finite element model is kept constant. This is based on assumptions that the stiffness of the wing is dominated by the aluminum-alloy insert and the mass distribution of the wing is significantly changed due to plastic foams covering the aluminum-alloy insert. This finite-element plate model predicts natural vibration modes of the wing that compare well with the experiment. The first three modal frequencies computed by using the finite element model are 21.8, 78.1, and 126 Hz and corresponding values measured in the experiment are 21.6, 79.7, and 121 Hz, respectively.

This is the first time a shell/plate FE model has been directly coupled with the Euler/Navier-Stokes equations. As a result, the validity of the coupling approach will be verified by comparing the FE results with those from the previously well-validated modal analysis. In this calculation, the FE computations were made using 36 plate elements and the modal computations were made using the first six modes of the wing. Six elements each were assigned along the chordwise and spanwise directions, respectively. Figure 3 shows the identical displacement responses of the leading edge at the tip obtained by both FE and modal analyses for $M_\infty = 0.854$, p = 0.70 psi and $\alpha = 1.0$ deg. Dynamic aeroelastic computations were made setting a high value for the damping coefficient so that the final results would approach to steady state conditions. The VS approach was used to calculate nodal forces for both FE and modal analysis. Results in Fig. 3 demonstrate the validity of the coupling of plate elements with the Euler/Navier-Stokes equations. The FE approach gives displacements about 0.1 % higher than the modal approach. Such results are expected since the modal approach yields a structure that is stiffer than the actual one, whereas the FE approach represents the actual structural stiffness.

The accuracy of the results can depend on the type of interfaces between fluids and structures. In the following calculations the simple lumped load and the more accurate virtual surface interfaces are compared to each other and the results are shown in Fig. 4. The wing structure was modeled using 100 ANS4 elements. Ten elements each were assigned along the chordwise and spanwise directions, respectively. For a given dynamic pressure of 1.0 psi and initial acceleration of $1.0 \times 10^5$ inches/sec, the time history of total lift on the wing is presented in Fig. 4. The total lift obtained by integrating the pressure coefficients at CFD grid points is also shown in the figure. The total lift using CFD grid points is more accurate than those from VS and LL methods. Both VS and LL approaches obtain the total lift by summing the forces at the FE nodal points, which was transformed from the pressure coefficients through interfaces. The VS approach transfers pressure data more accurately than the LL approach. The LL approach shows that the response around peaks

deviates from the CFD solution. For this case the LL approach shows favorable agreement with the VS approach.

Aeroelastic responses were also computed for various dynamic pressures in order to predict flutter dynamic pressure and compared with the experment.[22] Figure 5 shows the stable, near neutrally stable, and unstable responses of wing tip displacements at the leading edge for dynamic pressures of 0.85, 0.80, and 0.75 psi for $M_\infty = 0.854$. The Navier-Stokes equations and the virtual surface interface are used to obtain the FE nodal force vector. From the responses shown in Fig. 5, the interpolated dynamic pressure for the neutrally stable condition is 0.79 psi. It is noted that the experimental dynamic pressure measured at the neutrally stable condition was 0.91 psi. Considering the lack of experimental pressure data on the wing and the error involved in modeling the wing as a plate with constant thickness, the result is a favorable prediction of the flutter dynamic pressure.

ENSAERO has capability of modeling both the Euler and Navier-Stokes equations. It is of interest to know the effect of the type of flow equations on aeroelastic responses. Such studies will lead to the right choice of methods. For this purpose computations are made at a high-transonic Mach number of 0.970. Figure 6 shows the comparison between the steady pressures obtained from Euler and Navier-Stokes solutions. Since the Mach number is high-transonic, viscous effects are dominant. As a result there are significant differences between the Euler and Navier-Stokes solutions near and behind the shockwave. The Navier-Stokes solutions predict lower negative pressures near the shock waves. The viscous effects on the integrated total lift is shown in Fig. 7. The influence of viscous effects on the aeroelastic responses are shown in Fig. 8. In this case, aeroelastic computations are made when the wing is pitching up to one degree angle of attack (AoA) at a pitch rate of 0.01. Because of the reduced aerodynamic loads, the tip response from the Navier-Stokes solution is lower than that from the Euler solution.

## Computations on Wing-Body Configuration

As stated in the introduction one of the main reasons for modeling structures directly by finite elements instead of modes is to extend the fluid/structure interaction computational capability to more complex structures. The procedures demonstrated in the previous section are not limited to simple wing configurations. In this section, results are demonstrated for general wing-body configurations where it is not trivial to pre-select modes.

The selected wing-body configuration shown in Fig. 9 was modeled using a H-O type grid topology using a grid size of 99 x 79 x 30. Earlier work indicated that this grid was adequate for transonic flow computations at moderate angles of attack.[23]

In order to study the effect of structural flexibility on the flow, aeroelastic computations were made for the above wing-body configuration. Both the body and wing are allowed to be flexible. The wing is modeled using 30 plate elements and the body is modeled using 90 shell elements. The FE layout is shown in Fig. 10. Symmetric boundary conditions are applied at the top and bottom body symmetry lines. All DOF are constrained along the wing-body junction. This results in a total of 646 DOF for structures. This FE capability is incorporated in ENSAERO Version 3.1 in a modular way. The skyline data structure is used for the global stiffness and mass matrices.

The structural properties required for the analysis results in frequencies that represent a typical transport type wing-body. Figure 11 shows the mode shapes of the first four modes. For the current structural property assumptions, the first four modes are dominated by wing modes. The present 148-node FE model of the wing-body configuration can compute up to 646 modes.

As stated earlier, an analytical moving grid capability is implemented in ENSAERO based on H-O topology. The grid generated by the code when both the wing and the body are deformed is shown in Fig. 12. It is noted that the singular planes upstream of the leading edge and downstream of the trailing edge are deformed according to the deformed shape of the configuration.

## Forced Motion of Flexible Configuration

In order to verify the coupling of the surface movement with the grid movement, computations are made by forcing the motion. Computations are made at $M_\infty = 0.90$, $\alpha = 0.0$ deg and a reduced frequency $k(= \omega c/U)$ equal to 0.50, allowing the configuration to deform in the first torsional mode of the wing. The wing undergoes a torsional mode such that the maximum torsional angle at the tip is 1 deg. The unsteady computations are started from the converged steady state solution and 2400 time steps per cycle of oscillation are required. This corresponds to a nondimensional computational time step size $\Delta\tau = 0.0058$. Figure 13 shows the wing sectional lifts for various sections. As expected, the magnitude of the sectional lift increases towards the tip. A periodic lift response is obtained within two cycles of oscillations.

Free Motion on Aeroelastic Configuration

In this section, aeroelastic computations are made on the flexible wing-body configuration by directly coupling the pressures computed solving the Navier-Stokes equations with the FE structural equations. The LL interface is used for this computation. The structural properties of the wing-body configuration are selected to represent a typical aircraft. It is assumed that the wing-root is 256 inches long and aeroelastic computations are made at a dynamic pressure of 1.0 psi.

Demonstration computations are made for a static aeroelastic case when the configuration is ramping up from 0 to 5 deg AoA at $M_\infty = 0.90$. The configuration is pitched up about the axis perpendicular to the wall and located at the leading edge of the wing-root. Starting from the steady state solution the configuration is pitched up at a rate of 0.0012 deg per time step. This pitch rate was adequate to obtain a stable and accurate solution. At every time step the static equilibrium position is obtained by solving the static aeroelastic equations. At the end of each time step a new field grid is generated that conforms to the deformed surface. Figure 14 shows the response of the leading edge of the tip section.

Computational Resources

The current Navier-Stokes version of ENSAERO runs at 380 MFLOPS on the CRAY C90 at Ames Research Center. To run a rigid case, the code requires 33 words of central memory per grid point and 7 microseconds of CPU time per time step per grid point. For the flexible case there is an additional memory requirement of 1000 words per node and CPU time of 25 microseconds per time step per node. A typical dynamic aeroelastic response such as that shown in Fig. 14 requires about 4 CPU hours and 8 million words of central memory.

## Discussions and Conclusions

A domain-decomposition computational procedure is developed to compute aeroelastic responses using the Navier-Stokes flow solutions directly coupled with finite-element structural equations. The procedure is demonstrated using plate/shell finite elements. Aeroelastic computations are made for a typical wing-body configuration. Based on this work the following conclusions can be made.

1. It is feasible to directly couple the finite-difference flow equations and finite-element structural equations to obtain accurate results, though each discipline is solved in a separate computational domain. This domain decomposition approach takes advantage of efficient methods developed for each individual discipline.
2. The use of finite-element structures in place of modal structures produces more accurate and detailed results.
3. There is an increase in the requirement of computational time (about 8 % ) and memory for FE structures compared to the modal structures (for modal structures memory requirement is negligible).
4. The present domain decomposition approach will be extended for non-linear structures.
5. This approach is suitable for parallel computers. Work is in progress at the Ames Research Center to implement ENSAERO on Intel iPSC/860 parallel computer under NASA's High Performance Computing and Communications (HPCC) Program.

## References


[1] Holst, T. L, Flores, J., Kaynak, U., and Chaderjian, N. , "Navier-Stokes Computations, Including a Complete F-16 Aircraft," Chapter 21, Applied Computational Aerodynamics, edited by P. A. Henne, Vol. 125, *Progress in Astronautics and Aeronautics*, AIAA, ISBN 0-930403-69-X, 1990.

[2] Yang, T. Y., *Finite Element Structural Analysis*, Prentice-Hall, Inc., Englewood Cliffs, New Jersey, 1986.

[3] Guruswamy, P. and Yang, T. Y., "Aeroelastic Time Response Analysis of Thin Airfoils by Transonic Code LTRAN2," *Computers and Fluids*, Vol. 9, No. 4, Dec. 1980, pp 409-425.

[4] Borland, C. J. and Rizzetta, D., "XTRAN3S–Transonic Steady and Unsteady Aerodynamics for Aeroelastic Applications, Volume I–Theoretical Manual," AFWAL-TR-80-3107, Dec. 1985.

[5] Guruswamy, G. P., Goorjian, P. M., and Merritt, F. J., "ATRAN3S–An Unsteady Transonic Code for Clean Wings," NASA TM 86783, Dec. 1985.

[6] Batina, J. T., Bennett, R. M., Seidal, D. A., Cunningham, S. R., and Bland, S. R. , "Recent Advances in Transonic Computational Aeroelasticity," NASA TM 100663, Sept. 1988.

[7] Guruswamy, G. P., "Unsteady Aerodynamic and Aeroelastic Calculations of Wings Using Euler Equations," AIAA *Journal*, Vol. 28, No. 3, March 1990, pp 461-469.

[8] Guruswamy, G. P., "Vortical Flow Computations on a Flexible Blended Wing-Body Configuration," AIAA *Journal* , Vol. 30, No. 10, Oct. 1992, pp 2497-2503.

[9] Guruswamy, G. P., "ENSAERO–A Multidisciplinary

Program for Fluid/ Structural Interaction Studies of Aerospace Vehicles," *Computing System Engineering*, Vol. 1, Nos. 2-4, 1990, pp 237-256.

[10] Bendiksen, O. O., "A New Approach to Computational Aeroelasticity," AIAA-91-0939-CP, Baltimore, MD April 1991 pp 1712-1727.

[11] Felker, F. F., "A New Method For Transonic Static Aeroelastic Problems," AIAA-92-2123-CP, Dallas, Texas, April 1992, pp 415-425.

[12] Zienkiewicz, O. C., *The Finite Element Method*, Third Edition, McGraw Hill Book Company (UK) Limited, Maindenhead, Berkeshire, England, 1977.

[13] Peyret, R. and Viviand, H., "Computation of Viscous Compressible Flows Based on Navier-Stokes Equations," AGARD AG-212, 1975.

[14] Obayashi, S, Guruswamy, G. P., and Goorjian, P. M., "Streamwise Upwind Algorithm for Computing Unsteady Transonic Flows Past Oscillating Wings," AIAA *Journal*, Vol. 29, No. 10, Oct. 1991, pp 1668-1677.

[15] Beam, R. and Warming, R. F., "An Implicit Finite-Difference Algorithm for Hyperbolic Systems in Conservation Law Form," *Journal of Computational Physics*, Vol. 22, No. 9, Sept. 1976, pp. 87-110.

[16] Pulliam, T. H., and Chaussee, D. S., "A Diagonal Form of an Implicit Approximate Factorization Algorithm," *Journal of Computational Physics*, Vol. 39, No. 2, Feb. 1981, pp 347-363.

[17] Baldwin, B. S. and Lomax, H. ,"Thin-Layer Approximation and Algebraic Model for Separated Turbulent Flows," AIAA Paper 78-257, Huntsville, Alabama, 1978.

[18] Degani, D. and Schiff, L. B., "Computation of Turbulent Supersonic Flows .Around Pointed Bodies Having Cross Flow Separation," *Journal of Computational Physics*, Vol. 66, No. 1, Sept. 1986, pp 173-196.

[19] Park, K. C., Pramono, E. Stanley, G. M. and Cabiness, H. A., "The ANS Shell Elements: Earlier Developments and Recent Improvements, " Analytical and Computational Models of Shells, Edited by Noor, A.K. et al, CED-Vol.3, ASME, New York, 1989, pp 217-240.

[20] Appa, K.,"Finite-Surface Spline, " J. of Aircraft, Vol. 26, No. 5, May 1989, pp. 495-496.

[21] Luh, R. C., Pierce, L. and Yip, D., "Interactive Surface Grid Generation," AIAA Paper 91-0796, Reno Nevada, Jan. 1991.

[22] Dogget, R. V., Rainey, A. G. and Morgan, H. G., "An Experimental Investigation of Aerodynamics Effects of Airfoil Thickness on Transonic Flutter Characteristics, " NASA TM X-79, 1959.

[23] Obayashi, S., Guruswamy, G. P., and Tu, E. L., "Unsteady Navier-Stokes Computations on a Wing-Body Configuration in Ramp Motion," AIAA-91-2865, New Orleans, Louisiana, August 1991.

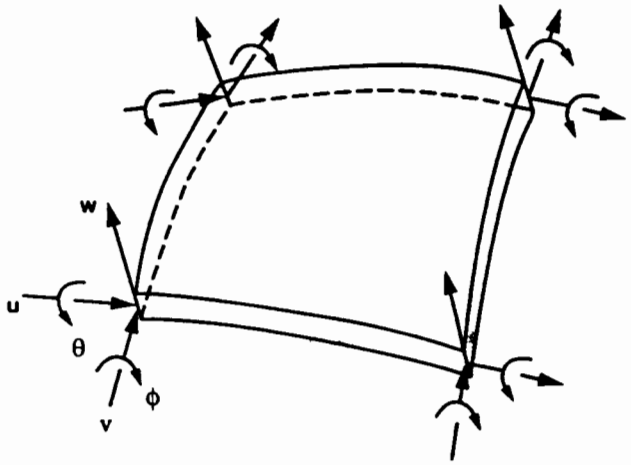


Fig. 1 Twenty degrees-of-freedom ANS4 shell/plate finite element.

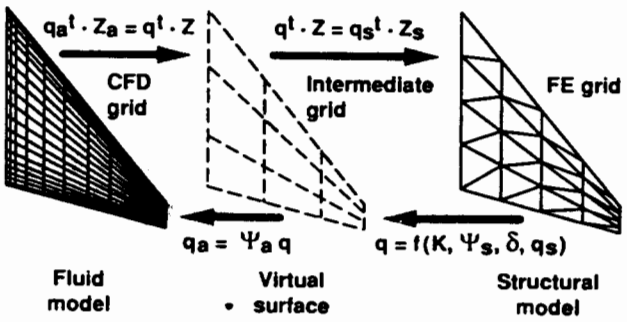


Fig. 2 Fluid-structure interfacing using virtual surface approach.

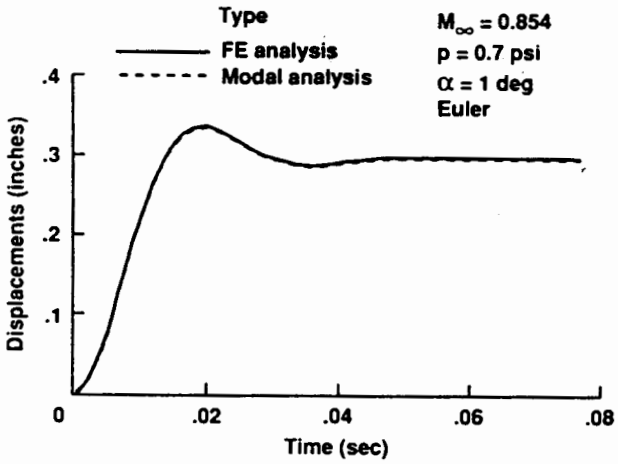


Fig. 3 Validation of finite element implementation in ENSAERO

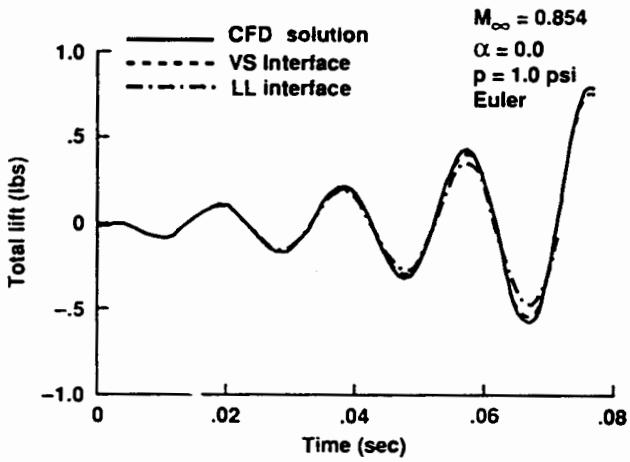


Fig. 4 Comparison of lumped load and virtual surface interfacing methods.

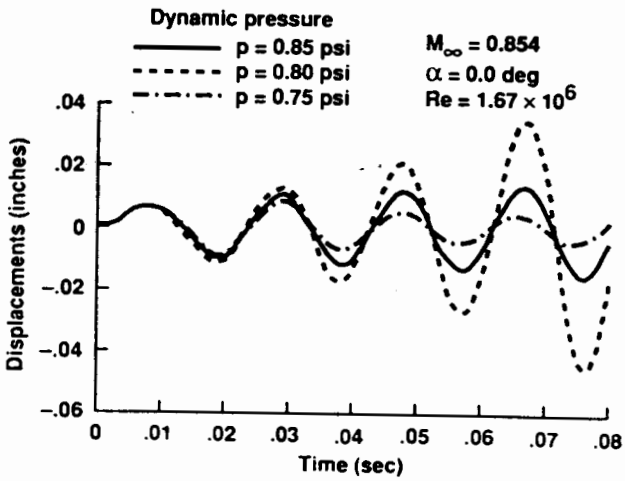


Fig. 5 Aeroelastic responses using a finite element model for structures.

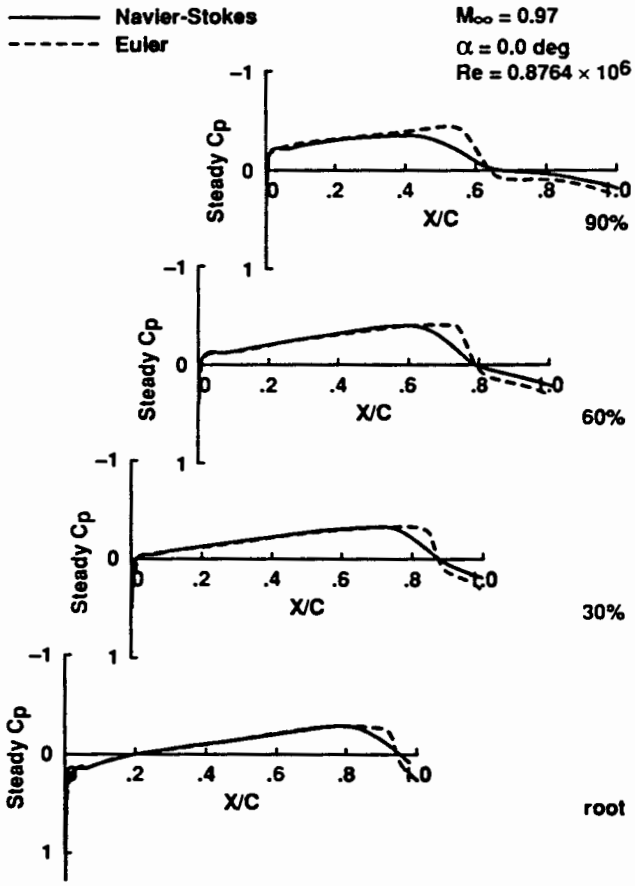


Fig. 6 Comparison of transonic steady pressures from Euler and Navier-stokes solutions.

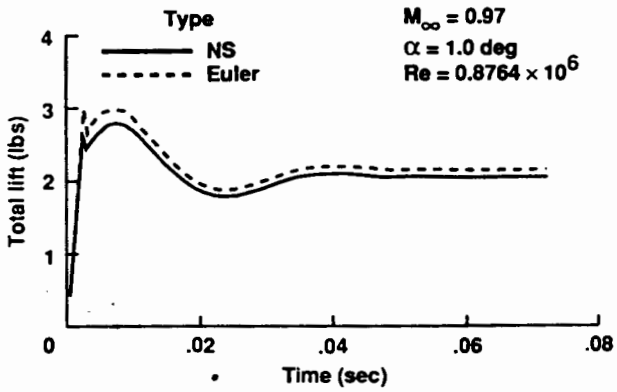


Fig. 7 Comparison of total lift from Euler and Navier-stokes solutions.

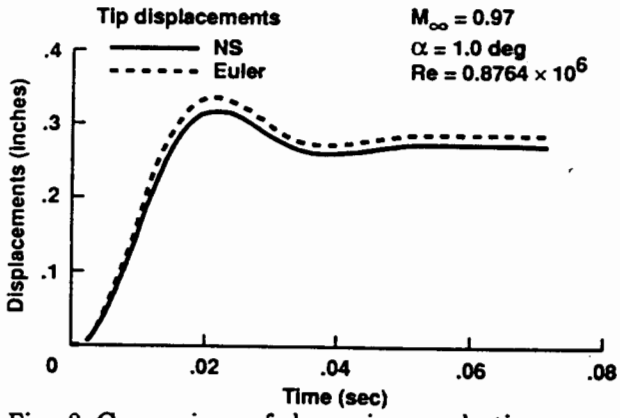


Fig. 8 Comparison of dynamic aeroelastic responses from Euler and Navier-stokes solutions

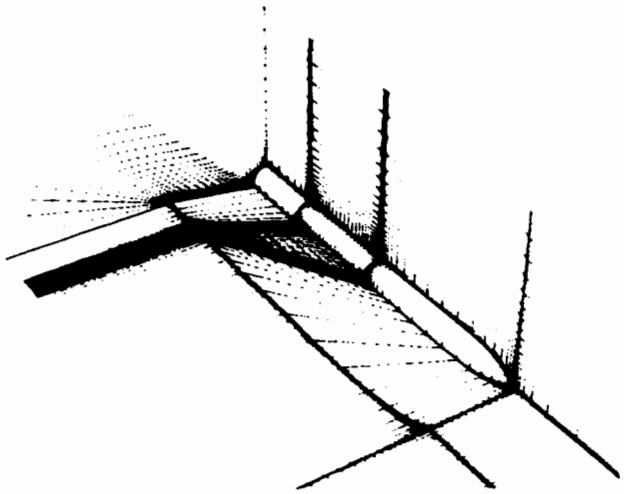

Fig. 9 Typical wing-body configuration with portions of surface and field physical grids.

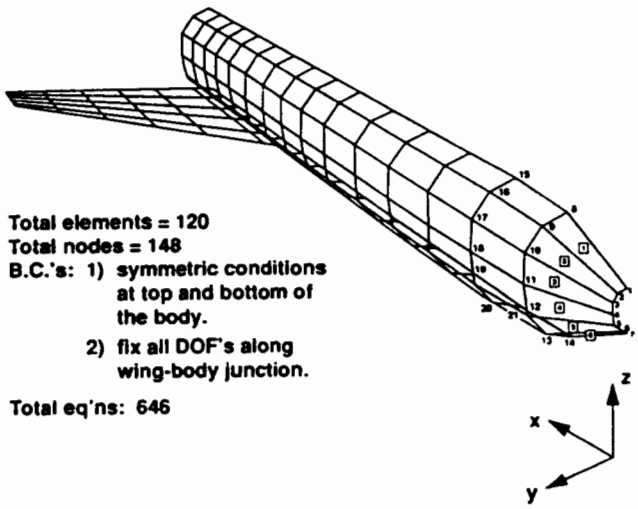


Fig. 10 Finite-element modeling of the wing-body configuration.

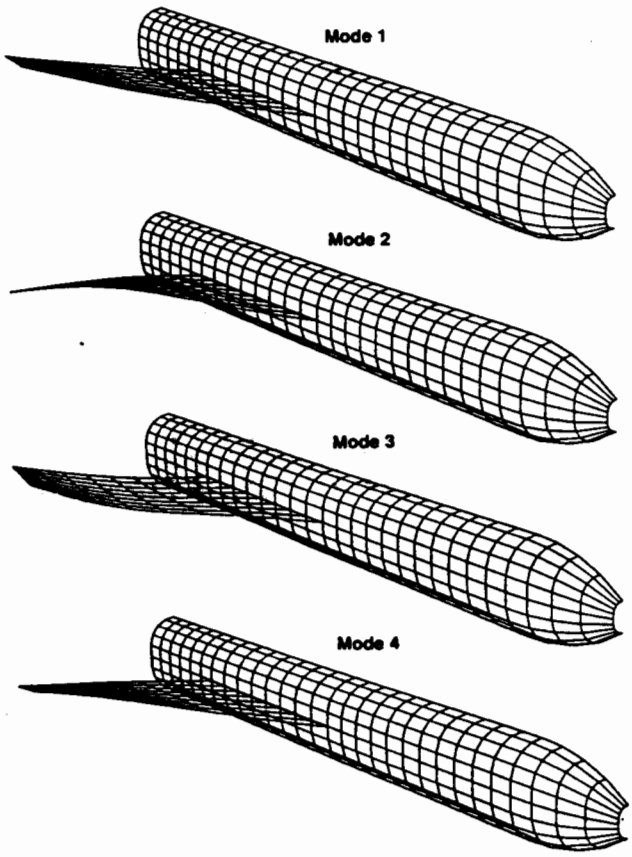


Fig. 11 First four natural modes of the wing-body configuration.

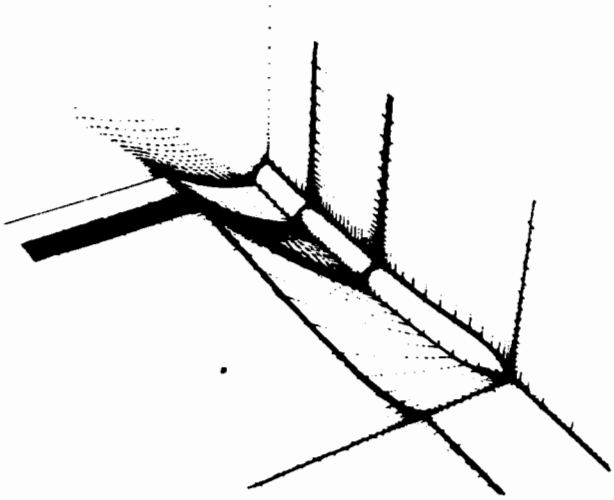

Fig. 12 Deformed surface and field grids.

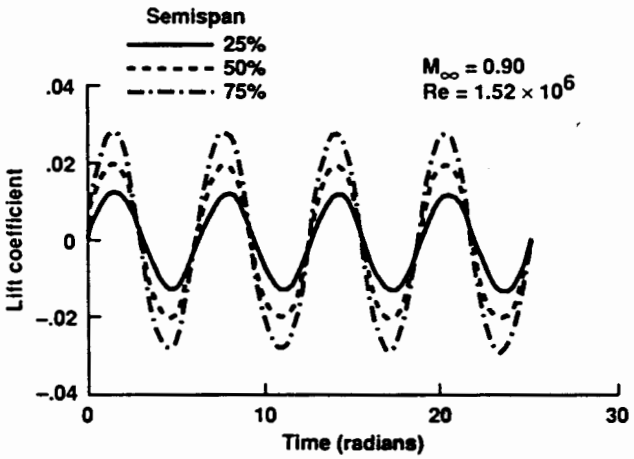


Fig. 13 Comparison of sectional lift responses for wing twisting mode.

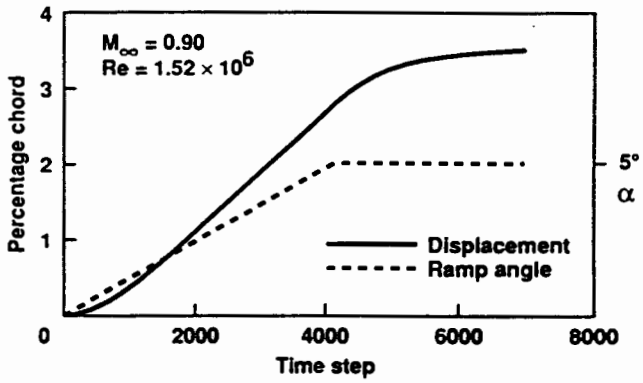


Fig. 14 Static aeroelastic displacements of wing-tip leading edge